Inorganic Chemistry

Article

pubs.acs.org/IC

Polyoxometalates Functionalized by Bisphosphonate Ligands: Synthesis, Structural, Magnetic, and Spectroscopic Characterizations and Activity on Tumor Cell Lines

Hani El Moll,[†] Wei Zhu,[‡] Eric Oldfield,*[,‡,§] L. Marleny Rodriguez-Albelo,[∥] Pierre Mialane,[†] Jérôme Marrot,[†] Neus Vila,[†] Israel Martyr Mbomekallé,[†] Eric Rivière,[⊥] Carole Duboc,[#] and Anne Dolbecq*[,†]

[†]Institut Lavoisier de Versailles, UMR 8180, Université de Versailles Saint-Quentin en Yvelines, 45 Avenue des Etats-Unis, 78035 Versailles cedex, France

[‡]Center for Biophysics and Computational Biology, University of Illinois at Urbana−Champaign, 607 South Mathews Avenue, Urbana, Illinois 61801, United States

[§]Department of Chemistry, University of Illinois at Urbana−Champaign, 600 South Mathews Avenue, Urbana, Illinois 6180, United States

[∥]Group of Materials Developed by Design, Division of Chemistry and Technology of Materials, Institute of Materials Research and Engineering (IMRE), University of Havana, Havana, 10400, Cuba

[⊥]Institut de Chimie Moléculaire et des Matériaux d'Orsay, UMR 8182, Université Paris-Sud, 91405 Orsay, France

[#]Département de Chimie Moléculaire, UMR 5250, Institut de Chimie Moléculaire de Grenoble, Université Jospeh Fourier Grenoble 1/CNRS, FR-CNRS-2607, BP 53, 38041 Grenoble cedex 9, France

Supporting Information

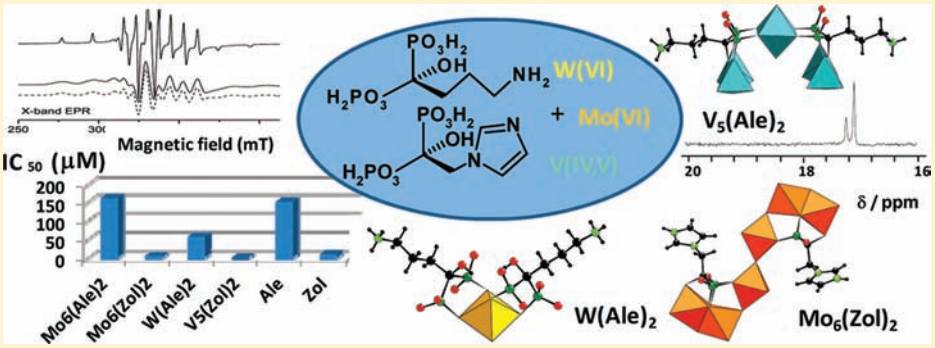

ABSTRACT: We report the synthesis and characterization of eight new Mo, W, or V-containing polyoxometalate (POM) bisphosphonate complexes with metal nuclearities ranging from 1 to 6. The compounds were synthesized in water by treating Mo^{VI}, W^{VI}, V^{IV}, or V^{V} precursors with biologically active bisphosphonates $H_2O_3PC(R)(OH)PO_3H_2$ (R = $C_3H_6NH_2$, Ale; R = $CH_2S(CH_3)_2$, Sul and R = $C_4H_5N_2$, Zol, where Ale = alendronate, Sul = (2-Hydroxy-2,2-bis-phosphono-ethyl)-dimethyl-sulfonium and Zol = zoledronate). $\mathbf{Mo_6(Sul)_2}$ and $\mathbf{Mo_6(Zol)_2}$ contain two trinuclear Mo^{VI} cores which can rotate around a central oxo group while $\mathbf{Mo(Ale)_2}$ and $\mathbf{W(Ale)_2}$ are mononuclear species. In $\mathbf{V_5(Ale)_2}$ and $\mathbf{V_5(Zol)_2}$ a central V^{IV} ion is surrounded by two V^{V} dimers bound to bisphosphonate ligands. $\mathbf{V_6(Ale)_4}$ can be viewed as the condensation of one $\mathbf{V_5(Ale)_2}$ with one additional V^{IV} ion and two Ale ligands, while $\mathbf{V_3(Zol)_3}$ is a triangular V^{IV} POM. These new POM bisphosphonates complexes were all characterized by single-crystal X-ray diffraction. The stability of the Mo and W POMs was studied by ^{31}P NMR spectroscopy and showed that all compounds except the mononuclear $\mathbf{Mo(Ale)_2}$ and $\mathbf{W(Ale)_2}$ were stable in solution. EPR measurements performed on the vanadium derivatives confirmed the oxidation state of the V ions and evidenced their stability in aqueous solution. Electrochemical studies on $\mathbf{V_5(Ale)_2}$ and $\mathbf{V_5(Zol)_2}$ showed reduction of V^{V} to V^{IV}, and magnetic susceptibility investigations on $\mathbf{V_3(Zol)_3}$ enabled a detailed analysis of the magnetic interactions. The presence of zoledronate or vanadium correlated with the most potent activity (IC_{50}∼1−5 μM) against three human tumor cell lines.

INTRODUCTION

Bisphosphonates (BPs) have been used to treat bone resorption diseases for almost 40 years but also have potent activity against some parasitic protozoa, and tumor cells.[1] The biologically active molecules having the general formula $H_2O_3PC(OH)(R)PO_3H_2$, possess a hydroxyl group that increases affinity of BPs for bone mineral, with R determining the potency of the drug. Compared

Received: May 15, 2012
Published: June 22, 2012

   dx.doi.org/10.1021/ic3010079 | Inorg. Chem. 2012, 51, 7921−7931

to etidronate (R = CH_3), compounds containing a basic primary nitrogen atom, such as alendronate (R = $(CH_2)_3NH_2$, noted Ale), were found to be 10−100 times more potent, while those with a nitrogen atom within a heterocyclic ring, such as zoledronate (R = $CH_2(C_3H_3N_2)$, herein noted as Zol) were up to 10,000× more potent.[2] Zoledronate is at present the most potent commercially available bisphosphonate drug and such BPs are generally referred to as NBPs, nitrogen-containing BPs. The cationic N center can also be replaced by a cationic S, and a previous study of sulfonium BPs showed that this category of BPs can have high activities in killing tumor cells.[3] Polyoxometalates (POMs) are discrete anionic metal−oxygen clusters which can be regarded as soluble oxide fragments. They are built from the connection of $\{MO_x\}$ polyhedra, M being a d-block element in high oxidation state, usually $V^{IV,V}$, $Mo^{V,VI}$, or W^{VI}.[4] These inorganic species exhibit great diversity in size, nuclearity, and shape which can be extended at will by the incorporation of suitable organic ligands.[5] POMs have been studied for some time for their biological activity.[6] For example, $[NH_3Pr^i]_6[Mo_7O_{24}]$, also known as PM-8, has exhibited growth suppression against Co-4 (human colon cancer), MX-1 (human breast cancer), and CAT (human lung cancer) cell lines,[7] and its photoreduced form suppressed the growth of several types of tumors, in vivo.[8] Covalent hybrid POMs have also been tested, for example $[Mo_8O_{26}L_2]^{4-}$ (L = alanine, glycylglycine,[9] proline[10]) octamolybdate derivatives, which inhibit the growth of HePG2 (hepatocellular carcinoma) and MCF-7 (breast cancer) cells. Preliminary growth inhibition tests also showed that organoimido derivatives of the Lindqvist polyoxomolybdates $[Mo_6O_{17}(NAr)_2]^{2-}$ (Ar = 3-NO_2−C_6H_4, 2-CH_3-4-NO_2−C_6H_3, 2-CH_3-5-NO_2−C_6H_3) have good inhibitory activities against K562 (human leucocythemia) cells, lower than the antitumor drug 5-fluorouracil but better than that of the parent $[Mo_6O_{19}]^{2-}$ POM at the same concentration.[11] The anticancer activity of polyoxotungstates including organotin[12] and organotitanium[13] substituted heteropolyoxotungstates bearing $\{Sn(CH_2)_2CN\}^{3+}$ or $\{CH_2CH(CH_3)C(O)OCH_3\}^{3+}$ and $\{CpTi\}^{3+}$ groups have also been reported. However, there are very few reports of studies on POMs in which the covalently grafted organic ligand itself possesses a recognized biological activity.[14]

In recent work, we initiated studies on the anticancer activity of hybrid molybdenum-bisphosphonate (alendronate) POMs[15] in which the activities of three Mo^V/Ale ($[Mo^V_4O_8(Ale)_2]^{4-}$, $[Mo^V_4O_8(O_3PC(C_{10}H_{14}NO)OPO_3)_2]^{6-}$, $[(Mo^V_2O_4)(H_2O))_4(Ale)_2]^{8-}$) and one Mo^{VI}/Ale ($[(Mo^{VI}_3O_8)_4(Ale)_4]^{8-}$, noted here $\mathbf{Mo_{12}(Ale)_4}$) molecules against three human tumor cell lines, MCF-7 (human breast cancer), NCI-H460 (lung large cell), and SF-268 (central nervous system glioblastoma), were investigated, in vitro.[15] The Mo^V/Ale compounds had weak but measurable activity while $\mathbf{Mo_{12}(Ale)_4}$ had IC_{50} values of ∼10 μM, about four times the activity of the parent alendronate molecule on a per-alendronate basis. Furthermore, the low activity of the ligand-free $[Mo_7O_{24}]^{6-}$ POM seemed to indicate a synergistic effect.

Here, we report the results of an extensive study on the synthesis and characterization of a series of POM/BP complexes to determine which parameters govern the biological activity of these compounds. The nature of both the POM and the BP have been varied. However, as Mo^{VI} POMs have proven to be more active than Mo^V compounds,[15] we have focused our study here on Mo^{VI}/BP polyoxomolybdates, combining POM cores with various BPs reported in the literature (Scheme 1). Complexes with Mo nuclearities equal to 1 or 6 have been isolated.

Scheme 1. Formulas of the Bisphosphonates Used for This Study

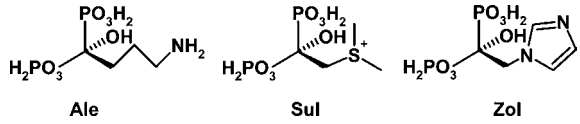

Additionally, a mononuclear W^{VI}/Ale POM and four new hybrid polyoxovanadates with BP ligands have been synthesized and characterized, to help clarify the relative effects of metal-versus-ligand. Electrochemical and magnetic measurements as well as electron paramagnetic resonance (EPR) spectroscopy are also reported for the magnetic polyoxovanadate compounds, to more fully characterize their structure and stability. And finally, the activity of ten such hybrid BP-POMs against three tumor cell lines is reported.

EXPERIMENTAL SECTION

Experimental Procedures and Characterization Data. $H_2O_3PC(C_3H_6NH_2)(OH)PO_3H_2$ (Ale),[16] $H_2O_3PC(C_3H_8S)(OH)PO_3H_2$ (Sul),[17] $H_2O_3PC(C_4H_5N_2)(OH)PO_3H_2$ (Zol),[18] $Na_2Rb_6[(Mo_3O_8)_4(O_3PC(C_3H_6NH_3)(O)PO_3)_4]\cdot 26H_2O$ ($\mathbf{Mo_{12}(Ale)_4}$),[15] and $Rb_{0.25}(NH_4)_{5.75}[(Mo_3O_8)_2O(O_3PC(C_3H_6NH_3)(O)PO_3)_2]\cdot 10H_2O$ ($\mathbf{Mo_6(Ale)_2}$)[19] were synthesized according to literature procedures.

$Rb_{0.75}(NH_4)_{5.25}[(Mo_3O_8)_2O(O_3PC(CH_2S(CH_3)_2)OPO_3)_2]\cdot 8H_2O$ ($\mathbf{Mo_6(Sul)_2}$). To a solution of $(NH_4)_6Mo_7O_{24}\cdot 4H_2O$ (0.660 g, 0.53 mmol) in 10 cm^3 of water was added Sul (0.362 g, 1.25 mmol). The solution was let stirring for 10 min. 2 M hydrochloric acid was added dropwise to pH = 3. The solution was then stirred for 1 h before addition of solid RbCl (0.500 g, 4.96 mmol). The solution was allowed to stir for another 1 h. The white powder was filtered and dried with ethanol and diethyl ether (yield: 0.690 g). The product was then dissolved in 25 cm^3 of 1 M CH_3COONH_4/CH_3COOH buffer, insoluble impurities were removed by centrifugation, and the solution was left to evaporate at room temperature. Colorless crystals were collected after 5 days. Yield 0.490 g (47% based on Mo). ^{31}P NMR (81 MHz, D_2O): δ 17.08 (s, 0.6 P), 16.95 (s, 1.4 P). ^1H NMR (200 MHz, D_2O): δ 3.80 (t, 2H, CH_2, $^3J_{HP}$ = 10.6 Hz), 2.91 (s, 4H, CH_3) and 2.85 (s, 2H, CH_3). Anal. Calc. (found) for $C_8H_{53}Mo_6N_{5.25}O_{39}P_4Rb_{0.75}S_2$ (1674.7): C 5.74 (5.68), H 3.19 (2.85), N 4.40 (4.27), S 3.83 (3.76), P 7.40 (7.34), Mo 34.37 (34.33), Rb 3.83 (3.37). IR (FTR): ν (cm^{-1}) = 1625 (w), 1419 (vs), 1276 (vw), 1138 (s), 1110 (w), 1086 (s), 1042 (s), 1003 (w), 980 (w), 909 (vs), 871 (vs), 814 (m), 720 (s), 675 (s), 612 (sh), 577 (vw), 558 (w), 531 (w), 487 (w), 454 (vw).

$(NH_4)_6[(Mo_3O_8)_2O(O_3PC(C_4H_6N_2)OPO_3)_2]\cdot 9H_2O$ ($\mathbf{Mo_6(Zol)_2}$). $(NH_4)_6Mo_7O_{24}\cdot 4H_2O$ (0.330 g, 0.265 mmol) and Zol (0.180 g, 0.625 mmol) were dissolved in 8 cm^3 of 0.5 M CH_3COONH_4/CH_3COOH. The solution was sealed in a 23 cm^3 Teflon-lined stainless steel reactor before heating to 130 °C over a period of 4 h, kept at this temperature for 20 h, then cooled to room temperature over a period of 36 h. The colorless crystals were collected by filtration. Yield 0.350 g (68% based on Mo). ^{31}P NMR (81 MHz, D_2O): δ 16.92 (s, 1 P), 16.61 (s, 1 P). ^1H NMR (200 MHz, D_2O): δ 8.83 and 8.76 (2 s, 1H, NCHN), 7.55 (s, 1H, NCHCHN), 7.32 (s, 1H, NCHCHN), 4.56 (t, 2H, NCH_2C, $^3J_{HP}$ = 9.5). Anal. Calc. (found) for $C_{10}H_{54}Mo_6N_{10}O_{40}P_4$ (1654.1): C 7.26 (7.36), H 3.29 (3.17), N 8.47 (8.39), P 7.49 (7.43), Mo 34.80 (34.52). IR (FTR): ν (cm^{-1}) = 1623 (w), 1580 (w), 1544 (w), 1423 (vs), 1135 (sh), 1082 (s), 1051 (s), 979 (m), 917 (s), 876 (vs), 819 (vw), 722 (m), 692 (s), 625 (m), 614 (m), 563 (m), 518 (m), 480 (m).

$(NH_4)_5Br[(Mo^{VI}O_2)(O_3PC(C_3H_6NH_3)(OH)PO_3)_2]\cdot 6H_2O$ ($\mathbf{Mo(Ale)_2}$). To a solution of $Na_2MoO_4\cdot 2H_2O$ (0.121 g, 0.50 mmol) in 10 cm^3 of 1 M CH_3COONH_4/CH_3COOH buffer was added Ale (0.249 g, 1.00 mmol). The solution was stirred for 10 min then 2 M sodium hydroxide added dropwise to pH = 7.5. The solution was then stirred for a further 1 h before addition of solid tetra-*n*-butylammonium bromide (TBABr, 0.300 g, 0.93 mmol). The solution was allowed to stir for another 1 h and the white powder filtered off, and the solution was left to evaporate at

dx.doi.org/10.1021/ic3010079 | Inorg. Chem. 2012, 51, 7921−7931

room temperature. Although TBA is not present in the product, addition of TBABr is important as it improves the yield of the synthesis and the quality of the crystals. Colorless crystals were collected after 5 days. Yield 0.380 g (85% based on Mo). Anal. Calc. (found) for $C_8H_{50}BrMoN_7O_{22}P_4$ (896.3): C 10.72 (11.44), H 5.62 (5.57), N 10.93 (11.26), Br 8.91 (7.88), Mo 10.70 (11.43), P 13.82 (14.51). IR (FTR): ν (cm^{-1}) = 1457 (s), 1405 (vs), 1145 (w), 1110 (s), 1040 (m), 1001 (sh), 966 (m), 948 (vw), 903 (m), 876 (s), 804 (w), 687 (m), 602 (vw), 567 (w), 524 (vw), 478 (m), 447 (vw), 440 (w), 487 (w).

*$(NH_4)_{4.5}Cs_{0.5}Cl[(W^{VI}O_2)(O_3PC(C_3H_6NH_3)(OH)PO_3)_2]\cdot 7H_2O$ (**W(Ale)$_2$**).* $Na_2WO_4\cdot 2H_2O$ (0.164 g, 0.50 mmol), Ale (0.249 g, 1.00 mmol), and CsCl (0.200 g, 1.18 mmol) were dissolved in 5 cm^3 of 1 M CH_3COONH_4/CH_3COOH buffer and 2 M sodium hydroxide added dropwise to pH = 7.5. The solution was sealed in a 23 cm^3 Teflon-lined stainless steel reactor before heating to 130 °C over a period of 4 h, kept at this temperature for 20 h, then cooled to room temperature over a period of 36 h. The white powder was filtered off and the solution left to evaporate at room temperature. Colorless crystals were collected after 5 days. Yield 0.210 g (41% based on W). Anal. Calc. (found) $C_8H_{52}ClCs_{0.5}N_{6.5}O_{23}P_4W$ (1017.2): C 9.44 (10.01), H 5.15 (5.01), N 8.95 (8.86), Cl 3.48 (3.47), Cs 6.53 (6.51), P 12.18 (12.34), W 18.07 (17.69). IR (FTR): ν (cm^{-1}) = 1557 (m), 1402 (vs), 1156 (w), 1122 (s), 1042 (s), 1004 (s), 960 (m), 937 (vw), 902 (m), 872 (s), 806 (w), 688 (m), 523 (sh), 478 (m), 408 (m), 393 (w), 361 (w).

*$Na_6Rb_2[(V_6O_{10}(H_2O)_2(O_3PC(C_3H_6NH_3)OPO_3)_4]\cdot 20H_2O$ (**V$_6$(Ale)$_4$**).* To a solution of $NaVO_3\cdot H_2O$ (0.067 g, 0.55 mmol) in 5 cm^3 of water was added Ale (0.124 g, 0.50 mmol) and RbCl (0.040 g, 0.33 mmol). The solution was stirred for 1 h then triethylamine added dropwise to pH = 5. The solution was then stirred for a further 1 h at 80 °C then left to evaporate at room temperature. Green crystals were collected after 5 days. Yield 0.050 g (25% based on V). Anal. Calc. (found) for $C_{16}H_{80}N_4Na_6O_{60}P_8Rb_2V_6$ (2151.1): C 8.94 (9.77), H 3.75 (3.93), N 2.61 (2.84), Na 6.41 (5.30), P 11.52 (12.31), Rb 7.94 (6.41), V 14.20 (13.80). IR (FTR): ν (cm^{-1}) = 1625 (s), 1503 (w), 1081 (w), 1038 (s), 1004 (vw), 975 (m), 903 (s), 667 (vw), 593 (w), 543 (w), 582 (w), 353 (m).

*$Na_3[V_3O_3(H_2O)(O_3PC(C_4H_6N_2)(OH)PO_3)_3]\cdot 12H_2O$ (**V$_3$(Zol)$_3$**).* To a solution of $NaVO_3\cdot H_2O$ (0.067 g, 0.55 mmol) in 5 cm^3 of water was added Zol (0.136 g, 0.50 mmol). The solution was stirred for 1 h; then triethylamine was added dropwise to pH = 5. The solution was stirred for a further 1 h at 80 °C and left to evaporate at room temperature. Pale blue platelets were collected after 5 days. Yield 0.190 g (79% based on V). Anal. Calc. (found) for $C_{15}H_{47}Na_3N_6O_{37}P_6V_3$ (1311.2): C 13.74 (13.42), H 3.61 (3.68), N 6.41 (6.23), Na 5.26 (5.14), P 14.17 (14.05), V 11.65 (11.35). IR (FTR): ν (cm^{-1}) = 1636 (m), 1577 (m), 1547(w), 1445 (w), 1404 (w), 1354 (w), 1314 (w), 1290 (w), 1099 (sh,s), 1080 (vs), 1053(sh, s), 996 (vs), 966 (s), 928 (m), 896 (w), 834 (m), 751 (w), 717 (w), 689 (w), 603 (s), 571 (s), 492 (m), 479 (m), 450 (m).

*$(NH_4)_2Rb_2[(V_5O_9(OH)_2(H_2O)(O_3PC(C_3H_6NH_3)OPO_3)_2]\cdot 8H_2O$ (**V$_5$(Ale)$_2$**).* $VOSO_4\cdot 5H_2O$ (0.190 g, 0.75 mmol), Ale (0.063 g, 0.25 mmol), and RbCl (0.150 g, 1.24 mmol) were dissolved in 8 cm^3 of 0.5 M CH_3COONH_4/CH_3COOH buffer and NH_3 33% was added dropwise to pH 6. The solution was sealed in a 23 cm^3 Teflon-lined stainless steel reactor before heating to 130 °C over a period of 4 h, kept at this temperature for 20 h, then cooled to room temperature over a period of 36 h. A small quantity of powder was filtered off and the solution left to evaporate at room temperature. After three days, black crystals of a non identified ligand-free vanadate were removed by filtration; then pale green crystals of $\mathbf{V_5(Ale)_2}$ were collected by filtration after 2 more days. Yield 0.040 g (21% based on V). Anal. Calc. (found) for $C_8H_{46}N_4O_{34}P_4Rb_2V_5$ (1292.0): C 7.44 (7.70), H 3.59 (3.34), N 4.33 (4.77), P 9.59 (9.85), Rb 13.23 (11.26), V 19.71 (19.66). IR (FTR): ν (cm^{-1}) = 1648 (s), 1401 (vs), 1173 (m), 1142 (m), 1100 (m), 1059 (s), 1032 (w), 982 (w), 919 (vs), 700 (vw), 641 (s), 513 (vw).

*$(NH_4)_{2.5}K_{1.5}[(V_5O_9(OH)_2(H_2O)(O_3PC(C_4H_6N_2)OPO_3)_2]\cdot 8H_2O$ (**V$_5$(Zol)$_2$**).* $VOSO_4\cdot 5H_2O$ (0.570 g, 2.25 mmol), Zol (0.205 g, 0.75 mmol) and KCl (0.450 g, 6.05 mmol) were dissolved in 24 cm^3 of 0.5 M CH_3COONH_4/CH_3COOH buffer and NH_3 33% was added dropwise to pH 6. The solution was sealed in a 125 cm^3 Teflon-lined stainless steel reactor before heating to 130 °C over a period of 4 h, kept at this temperature for 20 h, then cooled to room temperature over a period of 36 h. A small quantity of powder was filtered off and the solution left to evaporate at room temperature. After 3 days, dark crystals of a non identified ligand-free vanadate were removed by filtration, and pale green crystals of $\mathbf{V_5(Zol)_2}$ were collected by filtration after 2 more days. Yield 0.030 g (6% based on V). Anal. Calc. (found) for $C_{10}H_{42}N_{6.5}K_{1.5}O_{34}P_4V_5$ (1234.7): 9.72 (9.92), H 3.43 (3.31), N 7.37 (7.71), K 4.75 (4.40), P 10.03 (9.93), V 20.63 (20.06). IR (FTR): ν (cm^{-1}) = 1646 (s), 1418 (s), 1095 (sh), 1052 (s), 1040 (s), 982 (m), 905 (s), 698 (w), 667 (vw), 631 (m), 603 (m), 505 (w).

Infrared Spectra. Infrared spectra were recorded on an FTIR Magna 550 Nicolet spectrophotometer as pressed KBr pellets.

X-ray Crystallography. Data collection was carried out by using a Siemens SMART three-circle diffractometer for $\mathbf{Mo_6(Sul)_2}$, $\mathbf{Mo_6(Zol)_2}$, and $\mathbf{V_3(Zol)_3}$ and by using a Bruker Nonius X8 APEX 2 diffractometer for $\mathbf{Mo(Ale)_2}$, $\mathbf{W(Ale)_2}$, $\mathbf{V_6(Ale)_4}$, $\mathbf{V_5(Ale)_2}$, and $\mathbf{V_5(Zol)_2}$. Both were equipped with a CCD bidimensional detector using the monochromatized wavelength λ(Mo Kα) = 0.71073 Å. Absorption correction was based on multiple and symmetry-equivalent reflections in the data set using the SADABS program[20] based on the method of Blessing.[21] The structures were solved by direct methods and refined by full-matrix least-squares using the SHELX-TL package.[22] In all structures there are small discrepancies between the formulas determined by elemental analysis and those deduced from the crystallographic atom list because of the difficulty in locating all disordered water molecules (and sometimes the cations), a common feature found in other polyoxometalate structural investigations.[23] The data set for $\mathbf{V_3(Zol)_3}$, which has the largest "voids" and for which the sodium cations could not be located in the structure because of severe disorder, was corrected with the program SQUEEZE,[24] a part of the PLATON package of crystallography software used to calculate the solvent or counterion disorder, and to remove its contribution to the overall intensity data. In the structures of $\mathbf{Mo_6(Sul)_2}$, $\mathbf{Mo_6(Zol)_2}$, and $\mathbf{V_5(Ale)_2}$, NH_4^+ and H_2O could not be distinguished based on the observed electron densities; therefore, all the positions were labeled O and assigned the oxygen atomic diffusion factor. The program ADDSYM, a part of the PLATON package, detects a pseudo center of symmetry for the structure of $\mathbf{V_6(Ale)_4}$. However, the mean $|E^2 - 1|$ value is equal to 0.774, very close to the value expected for a noncentrosymmetric structure (0.736). Furthermore, the refinement in the centrosymmetric *Pnma* space group is not satisfactory and leads to a high R_1 value (0.25).

Crystallographic data are given in Table 1. Partial atomic labeling schemes, selected bond distances, and bond valence sum calculations[25] are reported in Supporting Information, Figures SI1–SI8. These calculations confirm the oxidation state of the Mo, W, and V ions as well as the presence of protons on some oxygen atoms.

Powder diffraction data was obtained on a Bruker D5000 diffractometer using Cu radiation (1.54059 Å).

NMR Measurements. ^{31}P NMR spectra were recorded in 5 mm tubes with ^1H decoupling by using a Bruker AC-300 spectrometer operating at 121.5 MHz. The ^{31}P NMR spectra shown in the Supporting Information were recorded on a Bruker AC-200 spectrometer. ^{31}P chemical shifts were referenced with respect to an external standard, 85% H_3PO_4. For all compounds ≈20 mg of sample was dissolved in D_2O (700 μL), except for $\mathbf{Mo_6(Zol)_2}$, which was dissolved in 700 μL of a mixture of D_2O (50%) and $NH_4OAc/HOAc$ buffer (50%, 1M). The concentrations thus varied in the 1–30 mM range.

Magnetic Measurements. The magnetic susceptibility measurements were carried out on polycrystalline samples using a Quantum Design MPMS SQUID magnetometer operating in the 300–2 K temperature range and 0–5.5 T. Susceptibility measurements were performed within an applied field of 1000 Oe. Pascal's constants were utilized to estimate diamagnetic corrections, the value in each case being subtracted from the experimental susceptibility data to give the molar magnetic susceptibility (χ_M).

Electrochemical Studies. Electrochemical data were obtained using an EG & G 273 A driven by a PC with M270 software. A one-compartment cell with a standard three-electrode configuration was used for cyclic voltammetry experiments. Prior to each experiment, solutions were deaerated thoroughly for at least 30 min with pure argon. A positive pressure of this gas was maintained during the experiment.

dx.doi.org/10.1021/ic3010079 | Inorg. Chem. 2012, 51, 7921–7931

Table 1. Crystallographic Data

	$Mo_6(Sul)_2$	$Mo_6(Zol)_2$	$Mo(Ale)_2$	$W(Ale)_2$	$V_6(Ale)_4$	$V_5(Ale)_2$	$V_5(Zol)_2$	$V_3(Zol)_3$
empirical formula	$C_8H_{53}Mo_6N_{5.25}O_{39}P_4Rb_{0.75}S_2$	$C_{10}H_{54}Mo_6N_{10}O_{40}P_4$	$C_8H_{20}BrMoN_7O_{19}P_4$	$C_8H_{52}ClCs_{0.5}N_{6.5}O_{23}P_4W$	$C_{16}H_{80}N_4Na_6O_{60}P_8Rb_2V_6$	$C_8H_{46}N_4O_{34}P_4Rb_2V_5$	$C_{10}H_{42}K_{1.5}N_{6.5}O_{34}P_4V_5$	$C_{15}H_{47}N_6Na_3O_{37}P_6V_3$
formula weight, g	1674.8	4963.8	818.0	1017.2	2151.1	1292.0	1234.7	1311.2
temperature, K	296	296	296	296	200	296	296	296
crystal system	triclinic	monoclinic	monoclinic	monoclinic	orthorhombic	orthorhombic	orthorhombic	monoclinic
space group	$P\bar{1}$	$P2_1/c$	$C2/c$	$C2/c$	$P2_12_12_1$	$Pna2_1$	$P2_12_12$	$P2_1/c$
a/Å	9.3739(8)	17.642(3)	17.6396(13)	17.526(3)	15.6504(7)	27.437(10)	14.357(6)	15.235(4)
b/Å	15.2154(13)	16.841(2)	10.3314(8)	10.382(2)	20.8102(10)	15.5104(4)	30.538(13)	12.776(3)
c/Å	17.8484(15)	17.587(3)	17.5641(14)	17.522(3)	23.9756(13)	9.9631(3)	9.420(4)	25.589(6)
α/deg	104.176(2)	90	90	90	90	90	90	90
β/deg	94.472(2)	108.198(3)	109.898(3)	109.726(6)	90	90	90	104.256(6)
γ/deg	96.615(2)	90	90	90	90	90	90	90
V/Å^3	2436.8(4)	4963.8(12)	3009.8(4)	3001.3(8)	7808.6(7)	4239.5(2)	4130(3)	4827(2)
Z	2	4	4	4	4	4	4	4
ρ_{calc}/g cm^{-3}	2.283	2.213	1.805	2.251	1.830	2.024	1.986	1.804
μ/mm^{-1}	2.567	1.715	2.060	4.852	2.235	3.599	1.510	0.910
data/parameters	13463/611	11398/628	4403/227	4384/245	22745/902	12111/525	7280/554	6328/554
R_{int}	0.0751	0.1161	0.0351	0.0252	0.0514	0.030	0.1060	0.047
GOF	1.035	0.962	1.071	1.153	1.071	1.089	0.989	1.019
R ($>2\sigma(I)$)	R_1[a] = 0.0524	R_1 = 0.0659	R_1 = 0.0297	R_1 = 0.0224	R_1 = 0.0902	R_1 = 0.0538	R_1 = 0.0595	R_1 = 0.0988
	wR_2[b] = 0.1481	wR_2 = 0.1485	wR_2 = 0.0833	wR_2 = 0.0645	wR_2 = 0.2598	wR_2 = 0.1650	wR_2 = 0.1533	wR_2 = 0.2751

[a] $R_1 = \sum||F_o| - |F_c||/\sum|F_o|$. [b] $wR_2 = [\sum w(F_o^2 - F_c^2)^2/\sum w(F_o^2)^2]^{1/2}$.

dx.doi.org/10.1021/ic3010079 | Inorg. Chem. 2012, 51, 7921−7931

Table 2. Human Tumor Cell Inhibition Data

	ref. for the synthesis	NCI-H460 IC_{50} [μM]	MCF-7 IC_{50} [μM]	SF-268 IC_{50} [μM]	average IC_{50} [μM]	average/BP IC_{50} [μM]
$Mo_{12}(Ale)_4$	15	9.2 ± 5.0	5.6 ± 0.4	5.0 ± 0.1	6.6 ± 3.1	26 ± 12
$Mo_6(Ale)_2$	19	48 ± 38	56 ± 0.0	130 ± 16	78 ± 45	160 ± 89
$Mo_6(Sul)_2$	this work	46 ± 0.3	35 ± 17	100 ± 11	61 ± 33	120 ± 66
$Mo_6(Zol)_2$	this work	2.4 ± 0.2	2.2 ± 0.1	3.0 ± 1.0	2.5 ± 0.6	5.0 ± 1.2
$Mo(Ale)_2$	this work	6.6 ± 2.2	9.4 ± 4.1	8.0 ± 0.8	8.0 ± 2.4	16 ± 4.9
$W(Ale)_2$	this work	11 ± 3.0	12 ± 3.6	63 ± 3.6	29 ± 27	57 ± 53
$V_6(Ale)_4$	this work	0.4 ± 0.0	0.5 ± 0.3	0.5 ± 0.2	0.5 ± 0.2	2.0 ± 0.7
$V_5(Ale)_2$	this work	0.5 ± 0.1	0.5 ± 0.2	0.8 ± 0.2	0.6 ± 0.2	1.2 ± 0.4
$V_5(Zol)_2$	this work	0.5 ± 0.1	0.4 ± 0.2	0.4 ± 0.0	0.4 ± 0.1	0.9 ± 0.2
$V_3(Zol)_3$	this work	0.3 ± 0.2	0.3 ± 0.0	0.3 ± 0.2	0.3 ± 0.1	0.9 ± 0.3
Ale		200 ± 43	130 ± 2.2	140 ± 13	150 ± 42	150 ± 42
Zol		8.1 ± 1.7	7.7 ± 2.6	12.4 ± 1.4	9.4 ± 2.8	9.4 ± 2.8
$Na_6[V^V_{10}O_{28}]$		0.2 ± 0.1	0.3 ± 0.2	0.3 ± 0.1	0.3 ± 0.1	NA

All experiments were performed at room temperature. A saturated calomel electrode was employed as reference electrode (SCE) whereas platinum gauze was used as a counter electrode. Both electrodes were separated from the bulk electrolyte solution via fritted compartments filled with the same electrolyte. The working electrode was a 3 mm OD glassy carbon disk (GC, Le Carbone de Lorraine, France). The pretreatment of this electrode before each experiment, adapted from the procedure of Keita and co-workers,[26] was as follows: (1) fine polishing using diamond pastes (DP Diamond-Struers) of decreasing grain size (15 min with a grain size of 6 μm, 15 min with a grain size of 3 μm and 30 min with a grain size of 1 μm). (2) The electrode then underwent two successive ultrasonic washings in ethanol and in water, respectively, for 5 min each. Results were very reproducible from one experiment to another with the slight variations observed over successive runs being attributed to the uncertainty associated with the detection limit of our equipment (potentiostat, hardware and software), and not to working electrode pretreatment.

EPR Experiments. Q-band EPR spectra were recorded at 30 K with a Bruker EMX, equipped with the ER-5106 QTW Bruker cavity and an Oxford Instruments ESR-900 continuous-flow helium cryostat. The X-band EPR spectra were recorded at 100 K with a Bruker EMX, equipped with the ER-4192 ST Bruker cavity and an ER-4131 VT for the liquid nitrogen experiments.

Cell-Growth Inhibition Assays. Cell growth inhibition assays were carried out exactly as described previously.[15] The IC_{50} values of Ale and $Mo_{12}(Ale)_4$ which had been measured in our first study[15] were redetermined in the same conditions as that used for the other compounds (Table 2).

RESULTS AND DISCUSSION

Structures. We first describe briefly the structure of the dodecanuclear and hexanuclear compounds reported previously which set the stage for a structural analysis of the new compounds, as well as a discussion of the cell-growth inhibition results. The $Mo_{12}(Ale)_4$ compound is built from the connection of four trimeric units (Supporting Information, Figure SI9) via two oxygen atoms, one from a P−O bond and one from a Mo−O bond and there is a central sodium ion.[19,27,28] The $Mo_6(Ale)_2$ complex (Figure 1c) has also been recently reported and studied for its photochromic[19,27] and catalytic properties.[28] This hexanuclear POM can be described as being essentially half of a dodecanuclear anion. Two trimeric units are linked via an Mo−O bond. Two conformers (hereafter labeled *A* and *B*, Supporting Information, Figure SI10) are observed.[19] In the *A* conformer, the six Mo^{VI} ions are approximately coplanar. The *B* conformer results from a rotation around the central oxygen atom, labeled Oi, of one of the trimeric unit (Figures 1 and Supporting Information, Figure SI10). In this conformer the

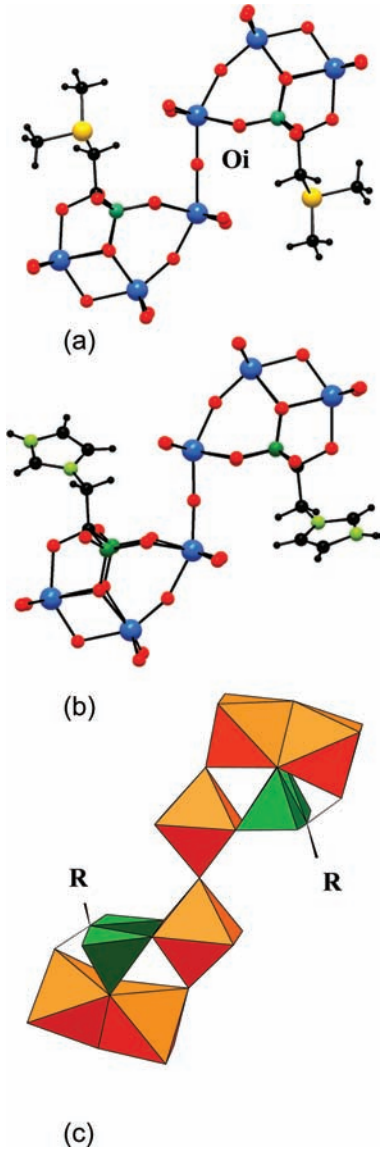

Figure 1. Ball and stick representation of the hexanuclear anions in (a) $Mo_6(Sul)_2$ and (b) $Mo_6(Zol)_2$; (c) polyhedral representation common to the Mo_6L_2 (L = Ale, Sul, Zol) POM frameworks, blue spheres = Mo, yellow spheres = S, dark green spheres = P, black spheres = C, light green spheres = N, red spheres = O, green tetrahedral = PO_3C, orange polyhedra = MoO_6.

dx.doi.org/10.1021/ic3010079 | Inorg. Chem. 2012, 51, 7921−7931

three Mo^{VI} ions of a trimeric unit are located in a plane perpendicular to the three Mo^{VI} ions of the other trimeric units. The molecular structures of $\mathbf{Mo_6L_2}$ (L = Sul, Zol) are very similar to that observed for the other hexanuclear $\mathbf{Mo_6L_2}$ species and has the *A* conformation, which is the conformation most frequently observed.[19,29] In $\mathbf{Mo_6(Sul)_2}$, the sulfur atoms of the sulfonium groups exhibit the expected pyramidal geometry (Figure 1a) and are located on one side or the other of the plane defined by the six Mo^{VI} ions. In $\mathbf{Mo_6(Zol)_2}$, the plane of the imidazolium groups is almost perpendicular to the plane of the POM core (Figure 1b). In the mononuclear $\mathbf{M(Ale)_2}$ (M = Mo, W) complexes, the central metal atom adopts a distorted octahedral coordination: two terminal oxo groups occupy *cis* vertices of the octahedron, four oxygen atoms of two different BP ligands occupy the four remaining vertices (Figure 2). A strong trans effect is observed resulting in a

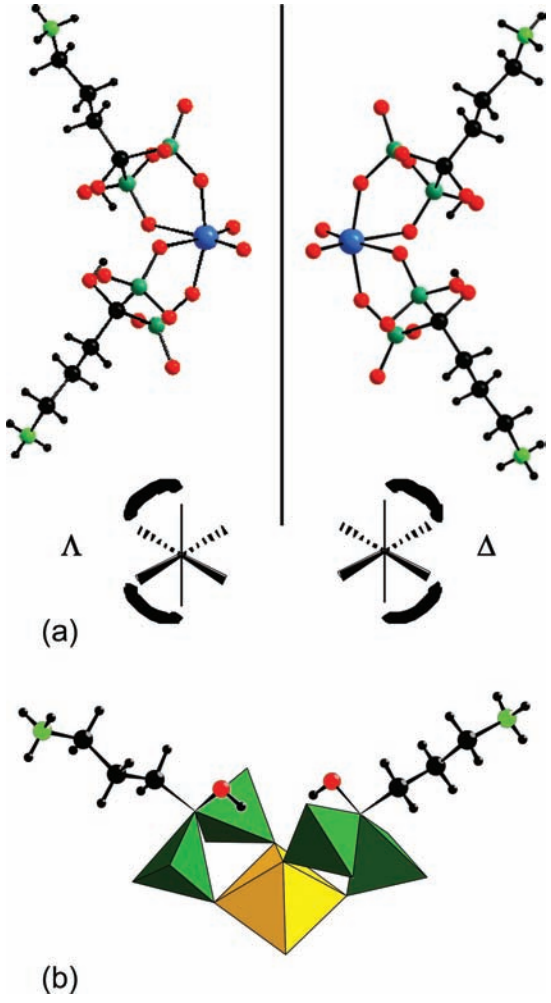

Figure 2. (a) Ball and stick representation of the Δ and Λ enantiomers of the mononuclear anions $\mathbf{M(Ale)_2}$ (M = Mo, W); (b) polyhedral representation; blue spheres = M, dark green spheres = P, black spheres = C, light green spheres = N, red spheres = O, yellow octahedra = MO_6 (M = Mo, W), green tetrahedra = PO_3C.

significant weakening of the Mo−O(P) bond trans to the Mo═O bond. These complexes possess neither a mirror plane nor a center of inversion and are thus chiral. The $\mathbf{M(Ale)_2}$ compounds crystallizes in a centrosymmetric space group, and both enantiomers, the so-called Δ and Λ isomers, are present in the unit-cell. Furthermore, unlike what is observed with the other Mo^{VI}/BP structures, the hydroxyl group of the alendronate ligand remains protonated and non coordinated.

The polyoxovanadates have nuclearities ranging from 3 to 6. The anion in $\mathbf{V_6(Ale)_4}$ is a cage complex in which three parallel planes can be defined: one plane has four V^V ions at the vertices of a pseudo rectangle, and the two planes located above and below contain one V^{IV} ion and four P atoms of the BP ligands (Figure 3a). The V^{IV} ions are in a distorted octahedral

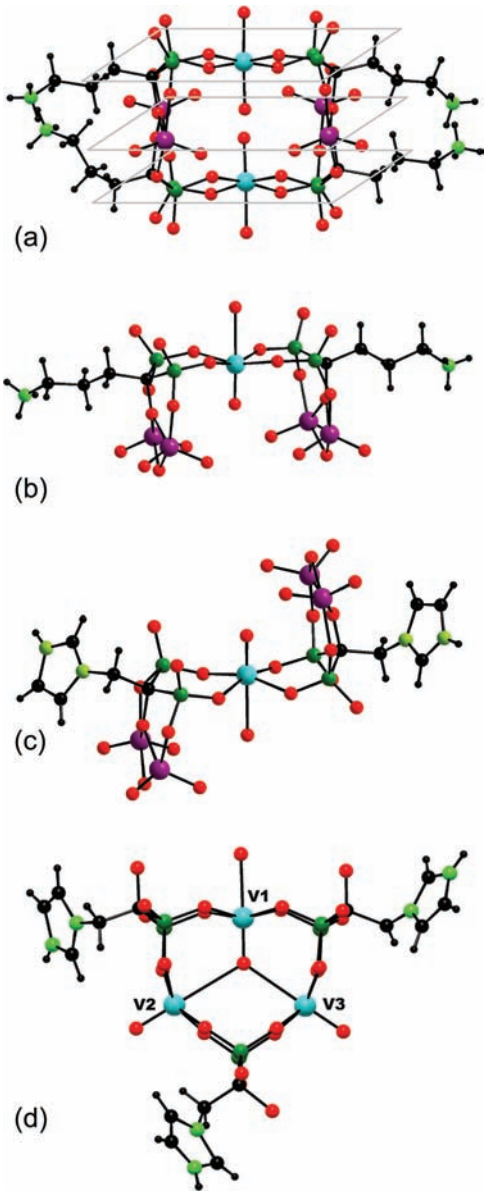

Figure 3. Ball and stick representation of the anions in (a) $\mathbf{V_6(Ale)_4}$, the gray diamonds highlight the three parallel planes (see text), (b) $\mathbf{V_5(Ale)_2}$, (c) $\mathbf{V_5(Zol)_2}$, and (d) $\mathbf{V_3(Zol)_2}$; cyan sphere = V^{IV}, purple spheres = V^V, dark green spheres = P, black spheres = C, light green spheres = N, red spheres = O.

coordination, with one short V═O bond trans to a long V−OH_2 bond. Four V−O(P) bonds with oxygen atoms from two different BP ligands complete the coordination sphere. The V^V ions adopt a distorted trigonal bipyramid coordination with two *cis* terminal V═O bonds, two V−O(P) bonds with two phosphonate groups from two BP ligands, and a V−O(C) bond with a deprotonated hydroxyl group of one of the alendronates.

dx.doi.org/10.1021/ic3010079 | *Inorg. Chem.* 2012, 51, 7921−7931

The -$(CH_2)_3NH_3^+$ chains of the four organic ligands are almost parallel. The anion in $\mathbf{V_5(Ale)_2}$ can be seen as a part of $\mathbf{V_6(Ale)_4}$, in which one V^{IV} ion connected to two BPs has been removed (Figure 3b). However, the penta-nuclear core appears more symmetric in $\mathbf{V_5(Ale)_2}$ than in $\mathbf{V_6(Ale)_4}$ (Supporting Information, Figure SI11). In $\mathbf{V_5(Ale)_2}$, the four V^V ions are closer in one direction of the rectangle, because of the existence of two bridging V−O(V) bonds which are not present in $\mathbf{V_6(Ale)_4}$, and a pseudosymmetry plane passing through the V^{IV} ion intersects the V^V pairs. In $\mathbf{V_5(Zol)_2}$, the alendronate ligand has been replaced by zoledronate, inducing a change in the conformation of the complex. In $\mathbf{V_5(Ale)_2}$ the plane containing the four V^V ions and the plane containing the V^{IV} ion and the four P of the BP ligands are parallel; this is not the case in the analogous complex $\mathbf{V_5(Zol)_2}$, in which these two planes intersect, two V^V ions being above the V^{IV} plane and two V^V ions below (Figure 3c). The anion in $\mathbf{V_5(Ale)_2}$ can thus be designated a *cis* isomer and the anion in $\mathbf{V_5(Zol)_2}$ a *trans* isomer. In $\mathbf{V_5(Zol)_2}$, one potassium ion connects two neighboring complexes (Supporting Information, Figure SI11). Three terminal oxo ligands (O═V^V, O═V^{IV}, O═P) of one complex, the same three terminal oxo groups of a neighboring complex together with a water molecule constitute its coordination sphere. The presence of this potassium ion may account for the *trans* configuration of the $\mathbf{V_5(Zol)_2}$ complex. In the trinuclear anion in $\mathbf{V_3(Zol)_3}$ three V^{IV} ions form an isosceles triangle (Figure 3d). Their octahedral coordination sphere is highly distorted. V2 and V3 have similar environment, with one short (~1.6 Å) V═O bond pointing outside the molecule, trans to a very long V−O (~2.6 Å) bond with the central O atom and four V−O(P) bonds of two tetradentate BP ligands. V1 has a terminal V═O bond with the central O atom trans to a V−OH_2 (~2.3 Å) bond with a water molecule, and four V−O(P) bonds with two zoledronate ligands. The hydroxyl group of the BP ligand remains protonated. The vanadium core possesses pseudo C_{2v} symmetry, with one mirror plane containing the three V ions, a C_2 axis passing through V1 and the central O atom, and a mirror plane perpendicular to the V plane and containing the C_2 axis. However, the whole molecule does not possess any symmetry element because of the position of the organic ligands. The trimeric V^{IV}/BP core present in $\mathbf{V_3(Zol)_3}$ has already been encountered in two complexes with etidronate (R = CH_3) ligands: the first was isolated from an aqueous solution of $[(C_2H_5)_2NH_2]_2VO(H_2L)$ (L = etidronate),[30] the second is the anionic unit of a lanthanide-vanadium-organic framework.[31] However both of these structures were severely disordered, unlike the structure of $\mathbf{V_3(Zol)_3}$.

Finally, the purity of these eight new crystalline phases has been checked on the bulk materials by comparison of the experimental powder X-ray diffraction data with the data calculated from the single X-ray diffraction analysis (Supporting Information, Figure SI12).

Synthesis and Characterization. The synthetic pathways are shown in Scheme 2. As observed by Sergienko et al.,[29] the oligomerization degree of the Mo^{VI} anionic complexes depends both on the Mo/L ratio and on the pH medium during synthesis, the counterion also having an important role in the ability to isolate complexes in the solid state. For a given Mo/L ratio, an increase of the pH results in the decrease in the extent of the oligomerization. $\mathbf{Mo_{12}(Ale)_4}$ was synthesized in water at room temperature at pH 3, from the reaction of Na_2MoO_4 with the BP reactants, as previously described. The presence of sodium ions is crucial as is the acidic pH value. In less acidic media, POMs with lower nuclearities are obtained. In a NH_4OAc/HOAc medium at pH 4.75, the hexanuclear $\mathbf{Mo_6L_2}$ (L = Ale, Sul, Zol) POMs are isolated while at pH 7.5, the mononuclear $\mathbf{Mo(Ale)_2}$ POM forms. Hydrothermal conditions were used in cases of products (or reactants) with low solubility, to increase product yield and crystallinity. Addition of cations such as K^+, Rb^+, or Cs^+ was also sometimes necessary, for similar reasons. The $\mathbf{V_6(Ale)_4}$ and $\mathbf{V_3(Zol)_3}$ polyoxovanadates were synthesized at room temperature from $NaVO_3$. Full or partial reduction of the V^V precursor is likely due to the presence of triethylamine. $\mathbf{V_6(Ale)_4}$ and $\mathbf{V_3(Zol)_3}$ were isolated under similar synthetic conditions, but have different molecular structures. $\mathbf{V_6(Ale)_4}$ contains two V^{IV} ions and four V^V ions, while in $\mathbf{V_3(Zol)_3}$, all the metal ions are V^{IV}. The $\mathbf{V_5(L)_2}$ (L = Ale, Zol) POMs were isolated under hydrothermal conditions from $VOSO_4$. In this case, air oxidation of the V^{IV} precursor led to the mixed valent polyoxovanadates which can be considered structurally to be part of the $\mathbf{V_6(Ale)_4}$ complexes.

All the POMs are soluble in water, but the polyoxovanadates were far less soluble than the Mo derivatives. ^{31}P NMR spectroscopy was used to determine whether structures characterized in the solid state were maintained in solution. This technique could, however, not be used for the magnetic polyoxovanadates as V^{IV} ions induce very large broadening of the nuclear lines.[32] Thus electrochemical and EPR characterizations were employed (see below). The ^{31}P NMR spectrum of the hexanuclear $\mathbf{Mo_6(Sul)_2}$ compound exhibits two singlets at 17.08 and 16.95 ppm with relative intensities 0.6:1.4 (Figure 4a). The same behavior is observed for $\mathbf{Mo_6(Zol)_2}$ with two singlets at 16.92 and 16.61 ppm with relative intensities 1:1. Only one singlet was expected if the structure observed in the solid state (Figure 2b) was retained in solution, corresponding to four equivalent phosphorus nuclei. The presence of another singlet close to the expected one has already been observed in other $\mathbf{Mo_6L_2}$ species and has been attributed to an equilibrium between the *A* and *B* conformers (Supporting Information, Figure SI10) following the dissolution of the POM. The attribution of each peak to one form or the other and a correlation between the different proportions of the *A* and *B* conformers and the nature of the BP cannot, however, be readily performed. The ^{31}P NMR spectrum of the mononuclear $\mathbf{Mo(Ale)_2}$ complex exhibits four set of signals when dissolved in water at room temperature: one sharp singlet at 18.08 ppm, which accounts for 70% of the total intensity, a doublet of doublets representing 9% (at 20.16, 19.93, 18.84, and 18.61 ppm) two singlets at 21.72 and 22.09, and a doublet at 19.24 and 19.43 ppm (Figure 4b). The effects of temperature on the evolution of this ^{31}P NMR spectrum indicate that an increase in temperature induces a broadening of the singlet at 18.08 ppm, together with the progressive disappearance of the other signals. At 275 K, the doublet of doublet represents 29% of the total intensity. This behavior can be explained by the presence of 5 species in solution: the expected mononuclear anion, three intermediate species resulting from its hydrolysis, and free alendronate ligands. The two alendronate ligands of the anion in $\mathbf{Mo(Ale)_2}$ are related by a C_2 axis but within each ligand, the P nuclei are not equivalent. The doublet of doublet can thus be attributed to this mononuclear species. The value of the coupling constant (J = 28.2 Hz) is in agreement with values observed for other Mo complexes.[17] The intensity of the singlet at 18.08 ppm increases upon addition of around 3 equiv of free alendronate in the solution, as does that of the doublet of doublets (Supporting Information, Figure SI13a), and no other signals are observed. The singlet at 18.08 ppm can thus be attributed to the free Ale. The similarities of the ^{31}P NMR spectra

dx.doi.org/10.1021/ic3010079 | *Inorg. Chem.* 2012, 51, 7921−7931

Scheme 2. Synthetic Pathways for the Dodecanuclear $Mo_{12}(Ale)_4$ POM, the Hexanuclear $Mo_6(Ale)_2$, $Mo_6(Sul)_2$, and $Mo_6(Zol)_2$ POMs, the Mononuclear $Mo(Ale)_2$ and $W(Ale)_2$ POMs, and the $V_6(Ale)_4$, $V_5(Ale)_2$, $V_5(Zol)_2$, and $V_3(Zol)_3$ Polyoxovanadates

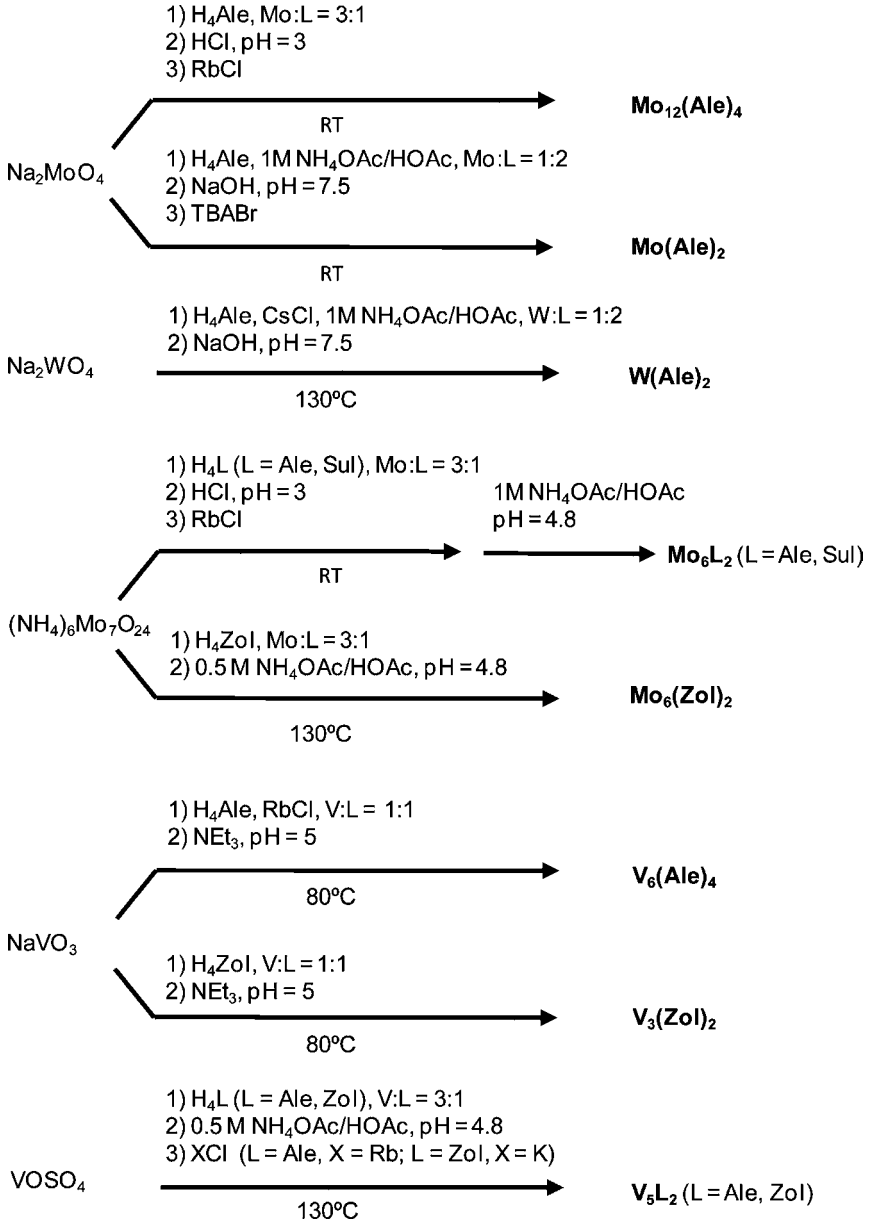

of $Mo(Ale)_2$ in physiological-like conditions[33] (Supporting Information, Figure SI13b), of a solution of $Mo(Ale)_2$ heated at 350 K and then cooled down to room temperature, and of the initial solution before being heated, show that (i) $Mo(Ale)_2$ also hydrolyzes in physiological-like conditions and (ii) surprisingly, the degradation is reversible. Finally, the ^{31}P spectrum of a solution of $W(Ale)_2$ in water at room temperature (Supporting Information, Figure SI13c) is close to that observed for $Mo(Ale)_2$ and indicates that $W(Ale)_2$ also hydrolyzes.

Magnetic Properties. All the molybdenum and tungsten compounds mentioned in this work are diamagnetic. With the vanadium compounds, the $V_5(Ale)_2$ and $V_5(Zol)_2$ complexes both possess a magnetically isolated V^{IV} center, while $V_6(Ale)_4$ contains two non-neighbor V^{IV} ions, with no strong delocalization of the d^1 electrons expected. Thus, the $V_3(Zol)_3$ compound is the only complex reported here possessing paramagnetic centers that might potentially have a significant magnetic interaction.

The magnetic behavior of $V_3(Zol)_3$ is shown in Figure 5. At 300 K, the $\chi_M T$ product, χ_M being the magnetic susceptibility for one mole of $V_3(Zol)_3$, is equal to 1.05 $cm^3\ mol^{-1}$ K, an expected value for three isolated V^{IV} centers ($\chi_M T$ = 1.05 $cm^3\ mol^{-1}$ K for g = 1.93). The $\chi_M T$ value is constant when the temperature decreases from 300 to 50 K, then increases when the sample is cooled further, reaching a $\chi_M T$ value of 1.15 $cm^3\ mol^{-1}$K at 2 K. This behavior is characteristic of predominantly weak ferromagnetic interaction. The $\chi_M T = f(T)$ curve has been fitted by direct diagonalization of an adapted Heinseberg–Dirac–Van Vleck Hamiltonian[34] taking into consideration the topology of $V_3(Zol)_3$. The anion in $V_3(Zol)_3$ possesses pseudo C_{2v} symmetry (see above), so the magnetic data can be modeled considering the system to be an isosceles triangle (Supporting Information, Figure SI14a) by using the following Hamiltonian:

$$\hat{H} = -J_1(\hat{S}_{V1}\hat{S}_{V2} + \hat{S}_{V1}\hat{S}_{V3}) - J_2(\hat{S}_{V2}\hat{S}_{V3})$$

dx.doi.org/10.1021/ic3010079 | Inorg. Chem. 2012, 51, 7921–7931

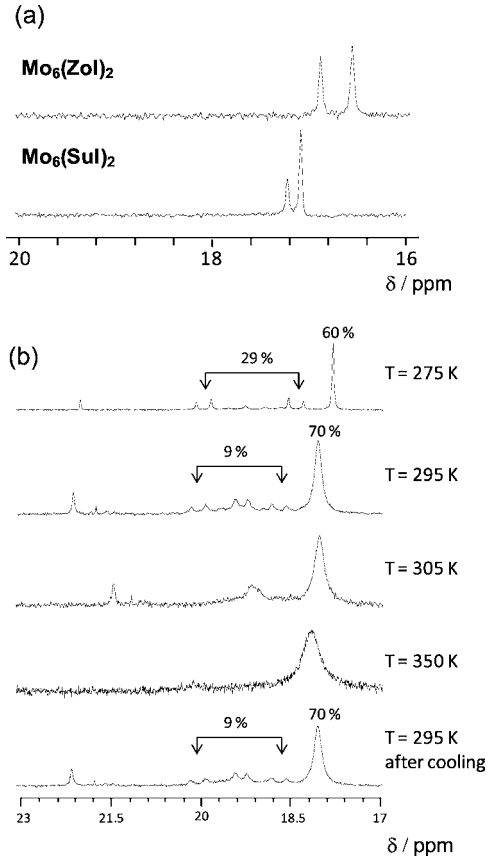

Figure 4. (a) ^{31}P NMR spectra of $\mathbf{Mo_6(Sul)_2}$, $\mathbf{Mo_6(Zol)_2}$ dissolved in D_2O at room temperature; (b) ^{31}P NMR spectrum of $\mathbf{Mo(Ale)_2}$ dissolved in D_2O from 275 to 350 K and of the same solution cooled down to 295 K after being heated at 350 K.

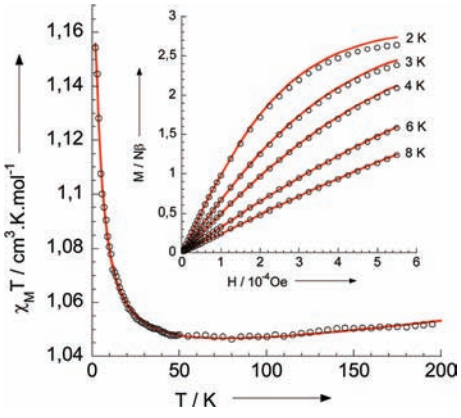

Figure 5. Thermal dependence of $\chi_M T$ for $\mathbf{V_3(Zol)_3}$. The solid line represents the best fitting result (see text). Inset: magnetization versus magnetic field at 2, 3, 4, 6, and 8 K; the solid lines correspond to the curves determined using the parameters deduced from the $\chi_M T = f(T)$ curve (see text).

with $S_{V1} = S_{V2} = S_{V3} = 1/2$. The best fitting parameters obtained are $J_1 = +1.56$ cm^{-1}, $J_2 = -1.06$ cm^{-1}, and $g = 1.92$ ($R = 1.0 \times 10^{-6}$),[35] assuming a temperature independent paramagnetism (TIP) value of 86×10^{-6} emu.mol^{-1}. The quality of the fit is much lower ($R = 2.3 \times 10^{-5}$) when the magnetic data are modeled using an idealized trigonal symmetry for the anion in $\mathbf{V_3(Zol)_3}$, and no improvement of the fit is observed when three independent coupling constants are considered. Moreover, the $M = f(H)$ curves recorded in the 2−8 K temperature range are satisfactorily reproduced by using the parameters deduced from the $\chi_M T = f(T)$ curve (Figure 5, inset) with the approximation that the anion in $\mathbf{V_3(Zol)_3}$ possesses C_{2v} symmetry. It can also be seen that, not unexpectedly, the weakest $|J|$ value (J_2) is found for the longest vanadium−vanadium distance (Supporting Information, Figure SI14a).

The V−O−P−O−V connection mode and magnetic properties observed in $\mathbf{V_3(Zol)_3}$ can be compared with those found in other phosphate-vanadium compounds in which no oxygen atom directly connect the paramagnetic centers. In these systems, both weak antiferromagnetic or ferromagnetic couplings have been found, and the J_1 and J_2 values determined here fall in the range of those reported previously.[36] Following the classification system proposed by Bond et al.,[36c] it can be seen that in $\mathbf{V_3(Zol)_3}$, ferromagnetic couplings are observed when the vanadium pairs adopt a boat configuration, while the antiferromagnetic interaction corresponds to a convex boat configuration (Supporting Information, Figure SI14b), although more detailed theoretical investigations into these observations would be welcome.[36b]

EPR Experiments. We recorded the X- (Figure 6) and Q- (Supporting Information, Figure SI15) band EPR spectra

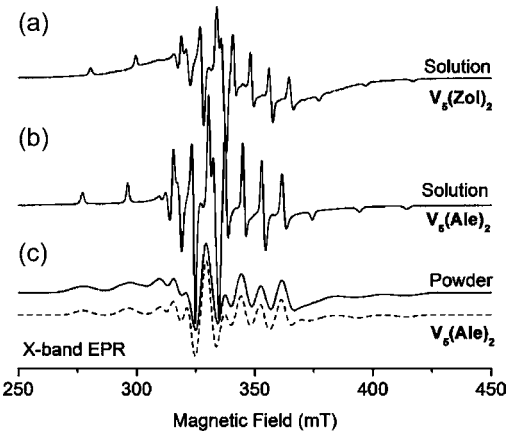

Figure 6. Experimental X-band EPR spectra recorded at 100 K in frozen aqueous ammonium acetate solutions of (a) $\mathbf{V_5(Zol)_2}$ and (b) $\mathbf{V_5(Ale)_2}$; (c) experimental (straight line) and simulated (dashed line) powder X-band EPR spectra recorded on $\mathbf{V_5(Ale)_2}$. EPR spin Hamiltonian parameters used for the simulation: $g_\parallel = 1.929$, $g_\perp = 1.969$, $A_{\parallel(V)} = 178$ MHz, $A_{\perp(V)} = 65$ MHz.

of polycrystalline $\mathbf{V_5(Ale)_2}$. The EPR spectra display an axial $S = 1/2$ signal consistent with a V^{IV} ion (d^1). Both transitions are split into eight lines due to the hyperfine interaction between the unpaired electron and the V nuclear spin ($I = 7/2$). The hyperfine coupling is larger along the parallel direction than along the perpendicular one, as expected for such V^{IV} compounds. In a frozen aqueous ammonium acetate solution, the X-band EPR spectrum of $\mathbf{V_5(Ale)_2}$ is similar to the powder one, except that the lines are much sharper (Figure 6b), because of reduced intermolecular dipolar interactions. The g-values in the EPR spectra of the powder and solution samples are the same ($g_\parallel = 1.929$, $g_\perp = 1.969$), consistent with the fact that the $\mathbf{V_5(Ale)_2}$ structure is retained in solution. In addition, the X-band EPR spectra of $\mathbf{V_5(Ale)_2}$ and $\mathbf{V_5(Zol)_2}$ in a frozen aqueous ammonium acetate solution are very similar (Figure 6), as expected.

The $\mathbf{V_6(Ale)_4}$ complex again displays an X-band powder EPR signal characteristic of an $S = 1/2$ system (Supporting

dx.doi.org/10.1021/ic3010079 | Inorg. Chem. 2012, 51, 7921−7931

Information, Figure SI16). However, the large broadening of the transition obscures the observation of hyperfine interactions and, consequently, the determination of the spin Hamiltonian parameters. The EPR spectrum of $\mathbf{V_6(Ale)_4}$ in water (Supporting Information, Figure SI16) is similar to that of the powder sample, strongly suggesting that the broadening of the line here arises from *intramolecular* dipolar interactions between the two V^{IV} ions present in $\mathbf{V_6(Ale)_4}$. In addition, these experiments show that the $\mathbf{V_6(Ale)_4}$ structure found in the solid state is maintained in solution.

Electrochemistry. We next investigated the electrochemical behavior of the most soluble vanadium based polyoxometalates $\mathbf{V_5(Ale)_2}$ and $\mathbf{V_5(Zol)_2}$. This study was challenging, because of the low solubility of these compounds, even though the CV experiments were performed in aqueous media at different pH values. A cyclic voltammogram of $\mathbf{V_5(Ale)_2}$ (Supporting Information, Figure SI15a), recorded in aqueous solution (1 M $CH_3COOLi + CH_3COOH$; pH = 5.00) at 50 mV s^{-1} starting at 0.6 V vs SCE shows on a first reduction scan a reversible cathodic peak located at $E^{\circ\prime}$ = +0.13 V, $E^{\circ\prime}$ being the apparent potential, assigned to the reduction of the vanadium centers (V^V/V^{IV}). This value is in accord with literature values, for example for the reduction of V^V centers in $[H_2V_{10}O_{28}]^{4}$.[37] As expected, scanning at higher scan rates (up to 100 mV s^{-1}) the intensity of the reduction current (I_{pc}) increased as the square root of the scan rate ($\nu^{1/2}$). No additional cathodic peaks were detected when scanning at more negative potentials. No significant differences were observed in the electrochemical behavior of $\mathbf{V_5(Ale)_2}$ when the study was carried out at pH = 3.0, and the same electrochemical response as seen with $\mathbf{V_5(Ale)_2}$ was obtained for $\mathbf{V_5(Zol)_2}$ (Supporting Information, Figure SI15b). The reduction of the four external V^V centers present within these structures can thus be observed in aqueous medium (pH 3 and pH 5), but the peak current is very small at low scan rates (<50 mV s^{-1}). It was thus not possible to obtain quantitative data (number of electrons) for this reduction, due presumably to the presence of organic moieties that surround the vanadium framework. Likewise, no evidence of the reduction of the internal V^{IV} centers could be detected by cyclic voltammetry, a probable consequence of the low current involved for the reduction of the V^V centers and the V^V/V^{IV} ratio equal to 4, that is, the expected intensity due to the reduction of the V^{IV} should be much lower than with V^V.

Cell-Growth Inhibition. We tested a series of Mo, W, and V-containing bisphosphonates against 3 human tumor cell lines: NCI-H460, MCF-7, and SF-268. Results are shown in Table 2 for each cell line in addition to the average IC_{50} values over all three cell lines, together with the average IC_{50} per bisphosphonate ligand, for comparison with free BP results. As can be seen in Table 2, the most active compounds are $\mathbf{Mo_6(Zol)_2}$, $\mathbf{V_6(Ale)_4}$, $\mathbf{V_5(Ale)_2}$, $\mathbf{V_5(Zol)_2}$, and $\mathbf{V_3(Zol)_3}$ which have (mean) IC_{50} values of 5, 2, 1.2, 0.9, and 0.9 μM, respectively (Table 2). Clearly then, all V compounds are active, but with the Mo and W compounds, potent activity is only found with the zoledronate-containing species, suggesting that here, the bisphophonate plays a larger part in tumor cell killing than in the V-containing systems. The high activity of $Na_6[V^V{}_{10}O_{28}]$ confirms that the enhanced activity comes from the inorganic part. However, for the Mo compounds there is also a clear effect of both the nature of the metal and of the structure of the POM. Indeed, for a given BP (here Ale), the W compound is less active than is the Mo analogue. Furthermore, the average activity per bisphosphonate ligand decreases in the following order: $\mathbf{Mo(Ale)_2} > \mathbf{Mo_{12}(Ale)_4} \gg \mathbf{Mo_6(Ale)_2} \sim$ Ale. All the Mo^{VI}/Ale complexes are more active than alendronate, with a 10-fold increase in potency for $\mathbf{Mo(Ale)_2}$. However, it remains to be determined if this effect is due to increased uptake into cells, more rapid dissociation within cells, or more subtle effects. Nevertheless, considering that $\mathbf{Mo_6(Zol)_2}$ is 30× more active than is $\mathbf{Mo_6(Ale)_2}$, it can be anticipated that the activity of an hypothetical complex with the formulas $\mathbf{Mo(Zol)_2}$ would be of the order of 500 nM.

CONCLUSIONS

We have synthesized eight new hybrid bisphosphonate POMs with Mo^{VI}, W^{VI}, $V^{IV,V}$ cores and nuclearities from 1 to 6. Our results show that bisphosphonate molecules of the general formula $H_2O_3PC(OH)(R)PO_3H_2$ (R = $(CH_2)_3NH_2$, $CH_2(C_3H_3N_2)$, $CH_2S(CH_3)_2$) can act as ligands in POM complexes with various compositions and geometries, confirming the great potentialities of this family of organic molecules for the synthesis of functionalized POMs.[15,19,27,28,38] The hydroxyl group of the BP ligand is found deprotonated in all the complexes, except in the trinuclear V^{IV} POM and the mononuclear Mo and W compounds. The absence of the additional P−O(M) (M = Mo, W) bond between the deprotonated hydroxo group and the metallic ion may account for the greater instability of the mononuclear species in aqueous medium, as evidenced by ^{31}P NMR spectroscopy. In the triangular V^{IV} anion, weak ferromagnetic interactions are observed between the closest V^{IV} ions, and a weak antiferromagnetic interaction occurs between the farthest magnetic ions. The most potent compounds in a tumor cell growth inhibition assay contained either vanadium or the most potent bisphosphonate, zoledronate, and had promising submicromolar IC_{50} values. In the future, synthetic efforts aimed at the preparation of mononuclear Mo complexes with zoledronate, as well as other potent bisphosphonate ligands, appear warranted, not least because the mevalonate pathway (in particular activity involving geranylgeranyl diphosphate) is now recognized as a therapeutic target for tumors having mutations in p53[39] and that the main site of action of zoledronate is in protein geranylgeranylation.[40]

ASSOCIATED CONTENT

Supporting Information

X-ray crystallographic details (CIF), partial atomic labeling scheme and bond valence summations for the eight new structures, representation of the anion in $\mathbf{Mo_{12}(Ale)_4}$ POMs, of the *A* and *B* conformers of the $\mathbf{Mo_6L_2}$ compounds, geometry of the pentanuclear cores in $\mathbf{V_6(Ale)_4}$, $\mathbf{V_5(Ale)_2}$, and $\mathbf{V_5(Zol)_2}$, ^{31}P NMR spectra of $\mathbf{Mo(Ale)_2}$, the magnetic core of $\mathbf{V_3(Zol)_3}$, powder EPR spectra recorded on $\mathbf{V_5(Ale)_2}$, X-band EPR spectra of $\mathbf{V_6(Ale)_4}$, cyclic voltammogramms of $\mathbf{V_5(Ale)_2}$ and $\mathbf{V_5(Zol)_2}$. This material is available free of charge via the Internet at http://pubs.acs.org.

AUTHOR INFORMATION

Corresponding Author

*E-mail: eo@chad.scs.uiuc.edu (E.O.), dolbecq@chimie.uvsq.fr (A.D.).

Notes

The authors declare no competing financial interest.

ACKNOWLEDGMENTS

This work was supported by CNRS, CNRS/TGE 3343, UVSQ, the French ANR (Grant ANR-11-BS07-011-01-BIOOPOM), and by the United States Public Health Service (NIH Grant

CA158191). Florian Molton is also gratefully acknowledged for recording the EPR spectra. The authors thank the TGE Réseau National de RPE interdisciplinaire, FR-CNRS-3443.

REFERENCES

(1) (a) Singh, A. P.; Zhang, Y.; No, J.-H.; Docampo, R.; Nussenzweig, V.; Oldfield, E. *Antimicrob. Agents Chemoth.* **2010**, *54*, 2987. (b) Mukherjee, S.; Huang, C.; Guerra, K.; Wang, K.; Oldfield, E. *J. Am. Chem. Soc.* **2009**, *131*, 8375. (c) Zhang, Y.; Cao, R.; Yin, F.; Lin, F. Y.; Wang, H.; Krysiak, K.; Mukkamala, D.; Houlihan, K.; Li, J.; Morita, C. T.; Oldfield, E. *Angew. Chem., Int. Ed.* **2010**, *49*, 1136. (d) Zhang, Y.; Cao, R.; Yin, F.; Hudock, M. P.; Guo, R. T.; Krysiak, K.; Mukherjee, S.; Gao, Y. G.; Robinson, H.; Song, Y.; No, J. H.; Bergan, K.; Leon, A.; Cass, L.; Goddard, A.; Chang, T. K.; Lin, F. Y.; Beek, E. V.; Papapoulos, S.; Wang, A. H.; Kubo, T.; Ochi, M.; Mukkamala, D.; Oldfield, E. *J. Am. Chem. Soc.* **2009**, *131*, 5153. (e) Song, Y.; Lin, F. Y.; Yin, F.; Hensler, M.; Rodrigues Poveda, C. A.; Mukkamala, D.; Cao, R.; Wang, H.; Morita, C. T.; Gonzalez Pacanowska, D.; Nizet, V.; Oldfield, E. *J. Med. Chem.* **2009**, *52*, 976.

(2) Widler, L.; Jaeggi, K. A.; Glatt, M.; Müller, K.; Bachmann, R.; Bisping, M.; Born, A.-R.; Cortesi, R.; Guiglia, G.; Jeker, H.; Klein, R.; Ramseier, U.; Schmid, J.; Schreiber, G.; Seltenmeyer, Y.; Green, J. R. *J. Med. Chem.* **2002**, *45*, 3721.

(3) Zhang, Y.; Hudock, M. P.; Krysiak, K.; Cao, R.; Bergan, K.; Yin, F.; Leon, A.; Oldfield, E. *J. Med. Chem.* **2007**, *50*, 6067.

(4) (a) Pope, M. T. *Heteropoly and Isopoly Oxometalates*; Springer-Verlag: New-York, 1983. (b) *Polyoxometalates: from Platonic Solids to Anti-Retroviral Activity*; Pope, M. T., Müller, A., Eds.; Kluwer Academic Publishers: Dordrecht, The Netherlands, 1994.

(5) Dolbecq, A.; Dumas, E.; Mayer, C. R.; Mialane, P. *Chem. Rev.* **2010**, *110*, 6009.

(6) (a) Rhule, J. T.; Hill, C. L.; Judd, D. A.; Schinazi, R. F. *Chem. Rev.* **1998**, *98*, 327. (b) Hasenknopf, B. *Front. Biosci.* **2005**, *10*, 275. (c) Crans, D. C.; Smee, J. J.; Gaidamauskas, E.; Yang, L. *Chem. Rev.* **2004**, *104*, 849. (d) Aureliano, M.; Crans, D. C. *J. Inorg. Biochem.* **2009**, *103*, 536.

(7) Yanagie, H.; Ogata, A.; Mitsui, S.; Hisa, T.; Yamase, T.; Eriguchi, M. *Biomed. Pharmacother.* **2006**, *60*, 349.

(8) Ogata, A.; Yanagie, H.; Ishikawa, E.; Morishita, Y.; Mitsui, S.; Yamashita, A.; Hasumi, K.; Takamoto, S.; Yamase, T.; Eriguchi, M. *Br. J. Cancer* **2008**, *98*, 399.

(9) Cindrić, M.; Novak, T. K.; Kraljević, S.; Kralj, M.; Kamenar, B. *Inorg. Chim. Acta* **2006**, *359*, 1673.

(10) Cartuyvels, E.; Van Hecke, K.; Van Meervelt, L.; Görller-Walrand, C.; Parac-Vogt, T. N. *J. Inorg. Biochem.* **2008**, *102*, 1589.

(11) Xue, S.; Chai, A.; Cai, Z.; Wei, Y.; Xiang, C.; Bian, W.; Shen, J. *Dalton Trans.* **2008**, 4770.

(12) (a) Wang, X.-H.; Dai, H.-C.; Liu, J.-F. *Trans. Met. Chem.* **1999**, *24*, 600. (b) Wang, X. H.; Liu, J. F. *J. Coord. Chem.* **2000**, *51*, 73.

(13) Wang, X.-H.; Liu, J. F.; Chen, Y.-G.; Liu, Q.; Liu, J.-T.; Pope, M. T. *Dalton Trans.* **2000**, 1139.

(14) Sarafianos, S. G.; Kortz, U.; Pope, M. T.; Modak, M. J. *Biochem. J.* **1996**, *319*, 619.

(15) Compain, J.-D.; Mialane, P.; Marrot, J.; Sécheresse, F.; Zhu, W.; Oldfield, E.; Dolbecq, A. *Chem.—Eur. J.* **2010**, *16*, 13741.

(16) Kubíček, V.; Kotek, J.; Hermann, P.; Lukeš, I. *Eur. J. Inorg. Chem.* **2007**, 333.

(17) Zhang, Y.; Hudock, M. P.; Krysiak, K.; Cao, R.; Bergan, K.; Yin, F.; Leon, A.; Oldfield, E. *J. Med. Chem.* **2007**, *50*, 6067.

(18) Martin, M. B.; Grimley, J. S.; Lewis, J. C.; Heath, H. T., III; Bailey, B. N.; Kendrick, H.; Yardley, V.; Caldera, A.; Lira, R.; Urbina, J. A.; Moreno, S. N. J.; Docampo, R.; Croft, S. L.; Oldfield, E. *J. Med. Chem.* **2011**, *44*, 909.

(19) El Moll, H.; Dolbecq, A.; Mbomekalle, I. M.; Marrot, J.; Deniard, P.; Dessapt, R.; Mialane, P. *Inorg. Chem.* **2012**, *51*, 2291.

(20) Sheldrick, G. M. *SADABS; program for scaling and correction of area detector data*; University of Göttingen: Göttingen, Germany, 1997.

(21) Blessing, R. *Acta Crystallogr.* **1995**, *A51*, 33.

(22) Sheldrick, G. M. *SHELX-TL version 5.03, Software Package for the Crystal Structure Determination*; Siemens Analytical X-ray Instrument Division: Madison, WI, 1994.

(23) (a) Sadakane, M.; Dickman, M. H.; Pope, M. T. *Angew. Chem., Int. Ed.* **2000**, *39*, 2914. (b) Zhang, C.; Howell, R. C.; Scotland, K. B.; Perez, F. G.; Torado, L.; Francesconi, L. C. *Inorg. Chem.* **2004**, *43*, 7691. (c) Zhang, Z.; Qi, Y.; Qin, C.; Li, Y.; Wang, E.; Wang, X.; Su, Z.; Xu, L. *Inorg. Chem.* **2007**, *46*, 8162. (d) Belai, N.; Pope, M. T. *Chem. Commun.* **2005**, *46*, 5760.

(24) van der Sluis, P.; Spek, A. L. *Acta Crystallogr., Sect. A.* **1990**, *46*, 194.

(25) Brese, N. E.; O'Keeffe, M. *Acta Crystallogr., Sect. B* **1991**, *47*, 192.

(26) Keita, B.; Nadjo, L. *J. Electroanal. Chem.* **1987**, *217*, 287.

(27) Compain, J.-D.; Deniard, P.; Dessapt, R.; Dolbecq, A.; Oms, O.; Sécheresse, F.; Marrot, J.; Mialane, P. *Chem Commun.* **2010**, *46*, 7733.

(28) Tan, H.; Chen, W.; Liu, D.; Feng, X.; Li, Y.; Yan, A.; Wang, E. *Dalton Trans.* **2011**, *40*, 8414.

(29) Sergienko, V. S. *Crystallogr. Rep.* **1999**, *44*, 877 , and references therein.

(30) Aleksandrov, G. G.; Sergienko, V. S.; Afonin, E. G. *Crystallogr. Rep.* **2001**, *46*, 53.

(31) Rocha, J.; Almeida Paz, F. A.; Shi, F.-N.; Ferreira, R. A. S.; Trindade, T.; Carlos, L. D. *Eur. J. Inorg. Chem.* **2009**, 4931.

(32) Bertini, I.; Turano, P.; Vila, A. J. *Chem. Rev.* **1993**, *93*, 2833.

(33) Margiotta, N.; Ostuni, R.; Piccinonna, S.; Natile, G.; Zanellato, I.; Boidi, C. D.; Bonarrigo, I.; Osella, D. *J. Inorg. Biochem.* **2011**, *105*, 548.

(34) MAGPACK software; Borras-Almenar, J. J.; Clemente-Juan, J. M.; Coronado, E.; Tsukerblat, S. B. *J. Comput. Chem.* **2001**, *22*, 985.

(35) $R = [\sum(\chi_M T_{calc} - \chi_M T_{obs})^2 / \sum(\chi_M T_{obs})^2]$.

(36) (a) Lisnard, L.; Dolbecq, A.; Mialane, P.; Marrot, J.; Rivière, E.; Borshch, S. A.; Petit, S.; Robert, V.; Duboc, C.; McCormac, T.; Sécheresse, F. *Dalton Trans.* **2006**, 5141. (b) Roca, M.; Amorós, P.; Cano, J.; Dolores Marcos, M.; Alamo, J.; Beltrán-Porter, A.; Beltrán-Porter, D. *Inorg. Chem.* **1998**, *37*, 3167. (c) Bond, M. R.; Mokry, L. M.; Otieno, T.; Thompson, J.; Carrano, C. J. *Inorg. Chem.* **1995**, *34*, 1894.

(37) Lee, U.; Joo, H-C; Park, K.-M.; Mal, S. S.; Kortz, U.; Keita, B.; Nadjo, L. *Angew. Chem., Int. Ed.* **2008**, *47*, 793.

(38) (a) Banerjee, A.; Raad, F. S.; Vankova, N.; Bassil, B. S.; Heine, T.; Kortz, U. *Inorg. Chem.* **2011**, *50*, 11667. (b) Breen, J. M.; Clérac, R.; Zhang, L.; Cloonan, S. M.; Kennedy, E.; Feeney, M.; McCabe, T.; Williams, D. C.; Schmitt, W. *Dalton Trans.* **2012**, *41*, 2918. (c) Niu, J.; Zhang, X.; Yang, D.; Zhao, J.; Ma, P.; Kortz, U.; Wang, J. *Chem.—Eur. J.* **2012**, *18*, 6759. (d) El Moll, H.; Dolbecq, A.; Marrot, J.; Rousseau, G.; Haouas, M.; Taulelle, F.; Rogez, G.; Wernsdorfer, W.; Keita, B.; Mialane, P. *Chem.—Eur. J.* **2012**, *18*, 3845.

(39) Freed-Pastor, W. A.; Mizuno, H.; Zhao, X.; Langerod, A.; Moon, S. H.; Rodriguez-Barrueco, R.; Barsotti, A.; Chicas, A.; Li, W.; Polotskaia, A.; Bissell, M. J.; Osborne, T. F.; Tian, B.; Lowe, S. W.; Silva, J. M.; Borresen-Dale, A. L.; Levine, A. J.; Bargonetti, J.; Prives, C. *Cell* **2012**, *148*, 244.

(40) Goffinet, M.; Thoulouzan, M.; Pradines, A.; Lajoie-Mazenc, I.; Weinbaum, C.; Faye, J. C.; Seronie-Vivien, S. *BMC Cancer* **2006**, *6*, 60.